

The PAH 3.4 micron feature as a tracer of shielding in the Orion Bar and NGC 6240

N. Thatte^{1*}, D. Rigopoulou^{1,2}, F. R. Donnan¹, I. Garcia-Bernete³, M. Pereira-Santaella⁴, B. Draine⁵
O. Veenema¹, B. Kerkeni^{6,7,8}, A. Alonso-Herrero³, L. Hermosa Muñoz³, G. Speranza⁴

¹ Department of Physics, University of Oxford, Keble Road, Oxford OX1 3RH, UK

² School of Sciences, European University Cyprus, Diogenes street, Engomi, 1516 Nicosia, Cyprus

⁴ Instituto de Física Fundamental, CSIC, Calle Serrano 123, 28006 Madrid, Spain

³ Centro de Astrobiología (CAB), CSIC-INTA, Camino Bajo del Castillo s/n, E-28692 Villanueva de la Cañada, Madrid, Spain

⁵ Department of Astrophysical Sciences, Princeton University, Princeton, NJ 08544-1001, USA

⁶ De Vinci Higher Education, De Vinci Research Center, 92916 Paris, France

⁷ Faculté des Sciences de Tunis, Laboratoire de Physique de la Matière Condensée, Université Tunis el Manar, Tunisia 2092

⁸ ISAMM, Université de la Manouba, La Manouba 2010, Tunisia

Accepted XXX. Received YYY; in original form ZZZ

ABSTRACT

We have carried out a detailed analysis of the 3.4 μm spectral feature arising from Polycyclic Aromatic Hydrocarbons (PAH), using JWST archival data. For the first time in an external galaxy (NGC 6240), we have identified two distinct spectral components of the PAH 3.4 μm feature: a shorter wavelength component at 3.395 μm , which we attribute to short aliphatic chains tightly attached to the aromatic rings of the PAH molecules; and a longer wavelength feature at 3.405 μm that arises from longer, more fragile, aliphatic chains that are weakly attached to the parent PAH molecule. These longer chains are more easily destroyed by far-ultraviolet photons ($>5\text{eV}$) and PAH thermal emission only occurs where PAH molecules are shielded from more energetic photons by dense molecular gas. We see a very strong correlation in the morphology of the PAH 3.395 μm feature with the PAH 3.3 μm emission, the latter arising from robust aromatic PAH molecules. We also see an equally strong correlation between the PAH 3.405 μm morphology and the warm molecular gas, as traced by H₂ vibrational lines. We show that the flux ratio PAH 3.395/PAH 3.405 < 0.3 corresponds strongly to regions where the PAH molecules are shielded by dense molecular gas, so that only modestly energetic UV photons penetrate to excite the PAHs. Our work shows that PAH 3.405 μm and PAH 3.395 μm emission features can provide robust diagnostics of the physical conditions of the interstellar medium in external galaxies, and can be used to quantify the energies of the photon field penetrating molecular clouds.

Key words: ISM:molecules – galaxies:ISM – techniques:imaging spectroscopy – infrared:galaxies – infrared:ISM – galaxies:individual:NGC 6240

1 INTRODUCTION

Polycyclic aromatic hydrocarbon (PAH) molecules are ubiquitously present in the Interstellar Medium (ISM) of our Galaxy and of star-forming galaxies (e.g. Smith et al. 2007; Galliano et al. 2008; Pereira-Santaella et al. 2010; Lai et al. 2023; Hernandez et al. 2023; Donnan et al. 2023; Rigopoulou et al. 2024) and Active Galactic Nuclei (AGN) (García-Bernete et al. 2022, 2024b; Zhang et al. 2024; Ramos Almeida et al. 2025) locally and at high redshifts (e.g. Chen et al. 2024; Spilker et al. 2023). They exhibit distinct infrared (IR) features at 3.3, 6.2, 7.7, 11.3 and 17 μm (e.g. Leger & Puget 1984) which are attributed to thermal emission by PAH molecules upon absorption of UV photons from their surrounding radiation fields.

PAH molecules consist of carbon and hydrogen atoms arranged in benzene ring structures (e.g. Tielens 2008). The emission bands

are believed to originate from the stretching and bending of the vibrational modes of the C-H and C-C bonds (e.g. Allamandola et al. 1985) with the smaller PAH molecules reaching high excitation temperatures and emitting strongly in the C–H stretching region encompassing the 3–4 μm regime (Ricca et al. 2012). PAHs are present in Photodissociation Regions (PDR) where they play a key role in heating the gas through the photoelectric phenomenon (e.g. Weingartner & Draine 2001). Understanding the nature, origin and evolution of PAHs across cosmic time and galaxy properties offers crucial insights into the interplay between galaxy evolution, dust, and gas.

The 3.3 μm PAH emission band is known to be an excellent tracer of small, neutral PAHs (e.g. Rigopoulou et al. 2021, 2024; Draine & Li 2007; Draine et al. 2021). In addition to the 3.3 μm band, a weaker band can also be observed around ~ 3.4 μm . The exact relationship between the 3.4 μm and 3.3 μm bands is unclear. The 3.4 μm band is often assigned to aliphatic side chains attached to PAH molecules (Duley & Williams 1981; Pauzat et al. 1999) although this idea has previously been disputed (e.g., Sandford et al. 1991).

* E-mail: niranjan.thatte@physics.ox.ac.uk

The $3.4\ \mu\text{m}$ PAH band has been seen to exhibit a lot of variability, depending on whether the carrier is purely aliphatic or attached to an aromatic ring system (Wexler 1967), and even shows some variability depending on the specific ring system to which it is attached, and the configuration of the resulting alkyl PAH molecule (e.g. Yang et al. 2013). Significant variation is also seen in astrophysical sources, where some planetary nebulae show a $3.4\ \mu\text{m}$ band which is stronger than the $3.3\ \mu\text{m}$ band (Hrivnak et al. 2007), despite it normally being the weaker of the two emission features. Other observations suggest the possibility of the $3.4\ \mu\text{m}$ band arising from an anharmonicity effect (Barker et al. 1987; Li & Draine 2012) or superhydrogenation (Sandford et al. 2013; Yang et al. 2020). In addition, Roche et al. (1996) suggested that the feature is more prominent in nitrogen rich objects. The comparative fragility of the aliphatic hydrocarbons is possibly the reason for the estimate of $<15\%$ of the carbon atoms responsible for emitting the PAH bands being in aliphatic form (Li & Draine 2012), however, this does not necessarily apply to the $3.4\ \mu\text{m}$ carriers observed in absorption (Chiar et al. 2013; Pendleton et al. 2025). In this paper, we will adopt the hypothesis that the $3.4\ \mu\text{m}$ band is attributed to aliphatic hydrocarbons. We will focus, in particular, on understanding the nature of the carriers, the relation between the 3.3 and $3.4\ \mu\text{m}$ bands and the use of the latter in probing the local ISM conditions. So far, detection of the PAH $3.4\ \mu\text{m}$ band has been limited to galactic sources (e.g., Roche et al. 1996; Jourdain de Muizon et al. 1990; Ohsawa et al. 2016) and a handful of IR luminous galaxies (e.g., Imanishi et al. 2010; Lai et al. 2023).

With the advent of JWST it is now possible to study PAH emission in a spatially resolved manner in a wide range of sources and environments. Observations with JWST/NIRSpec (covering the $1\text{--}5\ \mu\text{m}$ wavelength range) have paved the way for the study of the PAH 3.3 and $3.4\ \mu\text{m}$ emission features in galactic and extragalactic sources. Such observations have shown that the PAH $3.3\ \mu\text{m}$ and $3.4\ \mu\text{m}$ bands are observed in galaxies of the nearby Universe (e.g., Lai et al. 2023; García-Bernete et al. 2024a; Perna et al. 2024) and up to a redshift of four (the lensed galaxy SPT0418-47; Spilker et al. 2023), where only the $3.3\ \mu\text{m}$ band is detected with JWST/MIRI MRS. Finally, the PAH 3.3 and $3.4\ \mu\text{m}$ emission features have also been detected by JWST, through its Near Infrared Camera (NIRCam), in a number of galaxies at intermediate redshifts $z \sim 0.2\text{--}0.5$ in the Great Observatories Origins Deep Survey- South (GOODS-S; Lyu et al. 2025).

In this work, we focus on the emission from the weaker $3.4\ \mu\text{m}$ band and how the feature might be linked to the local physical conditions in the ISM of galaxies. We first investigate the nature of the aliphatic PAH $3.4\ \mu\text{m}$ emission band and then explore the conditions that might influence its presence and strength. In particular, we want to explore whether clouds of molecular hydrogen (H_2) might be shielding PAHs in strong UV radiation fields, as suggested by Rigopoulou et al. 2002; Roussel et al. 2007; Alonso-Herrero et al. 2020. For this purpose we employ archival observations of the Orion Bar, which offers unparalleled spatial resolution, and use this as a template to guide our investigations of nearby galaxies. In addition, we employ observations of the nearby Luminous Infrared Galaxy (LIRG) NGC 6240, A. Alonso-Herrero) which is well-known for its strong PAH and H_2 emission (e.g. Rigopoulou et al. 1999; Lutz et al. 2003; Alonso-Herrero et al. 2014; Hermosa Muñoz et al. 2025). The article is structured as follows: in Sect. 2, we give a brief description of the targets and the ensuing data analysis. In section 2.1.2 we discuss in detail the procedure we used for fitting and extracting the PAH 3.3 and PAH 3.4 features. In Sect. 3 we present theoretical spectra of molecules containing aliphatic side-groups, computed using Density Functional Theory (DFT). In Sect. 4 we analyse the spatial distribution of the features with a detailed discussion in Sect 5. Fi-

nally we present our conclusions in Sect. 6. Throughout the paper we use $H_0 = 70\ \text{km s}^{-1}\ \text{Mpc}^{-1}$, $\Omega_m = 0.3$, and $\Omega_\Lambda = 0.7$, unless otherwise stated.

2 OBSERVATIONS AND DATA REDUCTION

2.1 JWST Data

We used archival JWST NIRSpec IFU Spectroscopy to study the PAH emission features in the $3.2\text{--}3.6\ \mu\text{m}$ wavelength range. Data for NGC 6240 were obtained as part of the Guaranteed Time Observations (Program ID 1265, P.I. A. Alonso-Herrero) in the F290LP-G395H configuration. Data for the Orion Bar were obtained as part of the Early Release Science (ERS) programme (Program ID 1288, P.I. O. Berné), also with the F290LP-G395H configuration of NIRSpec in integral field mode. The NGC 6240 data were calibrated and reduced with the standard JWST NIRSpec pipeline, with one exception. We added an extra step between Stages 2 and 3 of the pipeline, correcting for residual bad, hot and dead pixels that had not been flagged by the pipeline, with a procedure similar to that described by García-Bernete et al. (2024a). For the Orion Bar, we used the Stage 3 data products from the MAST archive without any alterations.

2.1.1 NGC 6240 analysis

NGC 6240 is located at a distance of 108 Mpc, so each $0''.1$ IFS spaxel corresponds to 52 pc (NASA/IPAC Extragalactic Database). The aims of the data analysis were to recover the integrated flux in the PAH features in the range 3 to $4\ \mu\text{m}$ as well as a number of emission lines of molecular and ionized Hydrogen. The hydrogen recombination lines have been analysed and presented by Ceci et al. (2025) whereas an analysis of the molecular H_2 lines has been presented in Hermosa Muñoz et al. (2025) for NIRSpec and JWST/MIRI datasets, respectively. For the purposes of this work, we used the $\text{H}_2\ 0\text{--}0\ \text{S}(8)$ line of molecular Hydrogen (rest wavelength $5.053\ \mu\text{m}$), and the Pfund γ transition of ionized Hydrogen (rest wavelength $3.740\ \mu\text{m}$). We chose Pf γ over Pf β , as the Pf β transition is harder to isolate from nearby CO features, particularly in the nuclear regions. We also used $\text{H}_2\ 0\text{--}0\ \text{S}(8)$ instead of $\text{H}_2\ 0\text{--}0\ \text{S}(9)$ for the same reason. No correction for differential extinction was applied, given the relative proximity of the wavelengths of the features examined.

As described by Ceci et al. (2025) and Hermosa Muñoz et al. (2025), NGC 6240 exhibits very strong molecular hydrogen emission throughout its nuclear region, and relatively modest ionized hydrogen emission. Ceci et al. (2025) present a detailed kinematic analysis of several emission lines in the nuclear region of NGC 6240, including the $\text{H}_2\ 1\text{--}0\ \text{S}(1)$ line. They show that the molecular hydrogen emission exhibits two components in many spaxels within the NIRSpec IFU field-of-view, as do the ionized hydrogen features. Consequently, we used a double Gaussian fit (and a linear continuum) for all molecular hydrogen and ionized hydrogen lines in NGC 6240, using the `mpfit2gauss` routine. The `mpfit` library provides Levenberg-Marquardt least squares minimisation fits to user specified functions, we used it throughout our analysis for Gaussian and Drude profile fitting, with appropriate constraints.

2.1.2 PAH features

Before fitting the PAH features, we fitted and subtracted the emission from a number of lines in the same wavelength range as the PAH emission, namely the $\text{H}_2\ 1\text{--}0\ \text{O}(5)$ line ($\lambda_{\text{rest}} = 3.235\ \mu\text{m}$), the

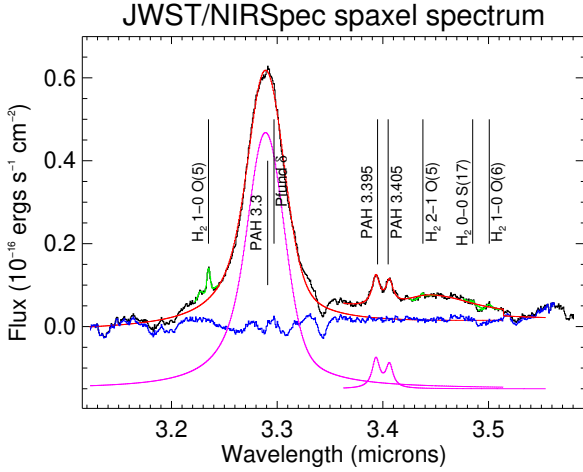


Figure 1. Rest-frame spectrum of a representative single spaxel in the nuclear region of NGC 6240 ($0^{\circ}1$ E, $0^{\circ}4$ S of the southern nucleus). Plotted flux is per spectral pixel. Median $1-\sigma$ error across the spectral range is 4.4% of plotted flux. Observed continuum subtracted spectrum in black, fits to the PAH features in red, fits to H_2 features in green, post-fit residual in blue. PAH Drude profiles overlaid in magenta (shifted for clarity, see Sec. 2.1.2 for details).

H_2 2–1 O(5) line ($\lambda_{\text{rest}} = 3.438 \mu\text{m}$), the H_2 0–0 S(17) line ($\lambda_{\text{rest}} = 3.485 \mu\text{m}$), and the H_2 1–0 O(6) line ($\lambda_{\text{rest}} = 3.500 \mu\text{m}$). A spectrum of a typical spaxel in the nuclear region with fits to these lines overlaid in green, is shown in Figure 1.

We fit the $3.3 \mu\text{m}$ PAH feature, using the combination of a Drude profile (Smith et al. 2007) and a Gaussian, plus a linear continuum. The Gaussian accounts for any Pf δ emission ($\lambda_{\text{rest}} = 3.297 \mu\text{m}$) just slightly redward of the PAH 3.3 peak, although the ionized hydrogen emission is weak compared to the PAH and H_2 features in the nuclear region of NGC 6240.

Figure 1 shows that the $3.4 \mu\text{m}$ PAH feature in NGC 6240 is clearly double-peaked. Although the double-peaked profile of the $3.4 \mu\text{m}$ feature has been previously observed in external galaxy spectra (e.g., Lai et al. 2023; Spilker et al. 2023), the two components have not been distinguished as separate features, and have typically been fit using a single Drude profile. For our analysis we follow the feature decomposition adopted by Peeters et al. (2024) for the PAH features in the $3.37\text{--}3.6 \mu\text{m}$ range in the Orion Bar and fit Drude profiles to five features centered at rest wavelengths of 3.395 , 3.405 , 3.425 , 3.464 and $3.516 \mu\text{m}$, with guess widths as per Table H.1 of Peeters et al. (2024). The fit includes a linear continuum spanning the wavelength range, and constraints on the 3.395 and $3.405 \mu\text{m}$ features to be blueward and redward of $3.4 \mu\text{m}$ respectively.

2.1.3 Orion Bar analysis

The Orion Bar is the outer region of the Orion Molecular Cloud, and is illuminated by the stars of Trapezium Cluster Peeters et al. (2024). The Orion Bar observations with JWST/NIRSpec cover nine slightly overlapping pointings. Detailed analysis of the NIRSpec data can be found in Berné et al. (2022); Peeters et al. (2024); Schroetter et al. (2024); Chown et al. (2024). Adopting the standard distance of 414 pc to the Orion Bar makes each $0^{\circ}1$ spaxel equal $2 \times 10^{-4} \text{ pc}$. We followed the same procedure as for NGC 6240 to fit the molecular hydrogen and ionized hydrogen emission lines, as well as the PAH features. The only exception was that there was no need to fit two

kinematic components to each hydrogen emission line, so we only fit single Gaussians. The resulting maps are shown in Figure 2.

3 THEORETICAL PAH SPECTRA

To gain further insight into the 3.3 and $3.4 \mu\text{m}$ PAH emission bands and, in particular, the nature of the double-peaked profile seen in the PAH $3.4 \mu\text{m}$ feature, here we examine DFT theoretical spectra of molecules containing aliphatic sidebands. Following the methodology described in Rigopoulou et al. 2021 and Kerkeni et al. 2022 we compute the IR spectra of PAH molecules containing methyl, ethyl and vinyl side-groups. To keep the computations simple we chose Coronene, a molecule with a small number of carbons ($N_c=24$) and computed DFT spectra of $C_{24}H_{12}$, $C_{24}H_{11}-CH_3$, $C_{24}H_{11}-CH_2-CH_3$ and $C_{24}H_{11}-CH=CH_2$. The computations presented here are not intended to be exhaustive but to give an indication of the strength and location of the PAH $3.4 \mu\text{m}$ feature in the presence of side-groups. We refer the reader to the works of Yang et al. (2020) and Cabezas et al. (2025) for a discussion of superhydrogenated and ring-containing aliphatic PAHs, respectively.

The structures and vibrational frequencies of the four molecules presented here were optimised with B3LYP/6-311++G(d,p) using Gaussian 16¹. Infrared spectra were computed from harmonic frequencies and intensities according to Barzaga et al. (2025). In Figure 3 we show the model emission spectra in the $3\text{--}4 \mu\text{m}$ range for neutral PAHs exposed to photons of 6 eV energy. We consider the full cascade model (for details see Rigopoulou et al. 2021 and references therein). It is evident from the spectra that the addition of ethyl/methyl side-groups shifts the peak of the $3.4 \mu\text{m}$ feature redward towards the observed $3.405 \mu\text{m}$ peak. Likewise, a peak blueward of $3.4 \mu\text{m}$ becomes prominent as the number of CH_3 side-groups decreases.

The bond dissociation energies (BDE) to remove the attached aliphatic side groups are 4.14 , 3.94 , and 4.51 eV for $C_{24}H_{11}-CH_3$, $C_{24}H_{11}-CH_2-CH_3$, and $C_{24}H_{11}-CH=CH_2$, respectively (e.g., Buragohain et al. (2020)). In the harsh conditions of an astronomical source, the chemical pathways might be different and perhaps there might be an intermediate product before the molecule completely loses the attached side groups. Of the three molecules considered here, vinyl side groups ($-CH=CH_2$) are more strongly bound and 4.51 eV is needed to remove the group from the parent molecule.

4 DO H_2 MOLECULAR CLOUDS SHIELD PAH MOLECULES?

In this Section we set out to investigate how the physical ISM conditions impact the presence and strength of the two components that make up the PAH $3.4 \mu\text{m}$ feature. We want to establish what sets the overall strength of the two components seen in Figure 1. In the pre-JWST era the double-peaked nature of the feature was not known and investigations were focused on the relation between aliphatic and aromatic stretches, which correspond to the PAH $3.4 \mu\text{m}$ and PAH $3.3 \mu\text{m}$ emission features, respectively. For instance, Yang & Li (2023) investigated the ratio PAH 3.3/PAH 3.4 in samples of Planetary Nebulae (PNs), Reflection Nebulae (RNs) and Photo-Dissociation Regions (PDR) and concluded that the aliphatic feature is stronger in UV-poor environments (they treat the PAH $3.4 \mu\text{m}$ as

¹ Gaussian 16, Revision C.01, M. J. Frisch et al., Gaussian Inc., Wallingford CT (2016).

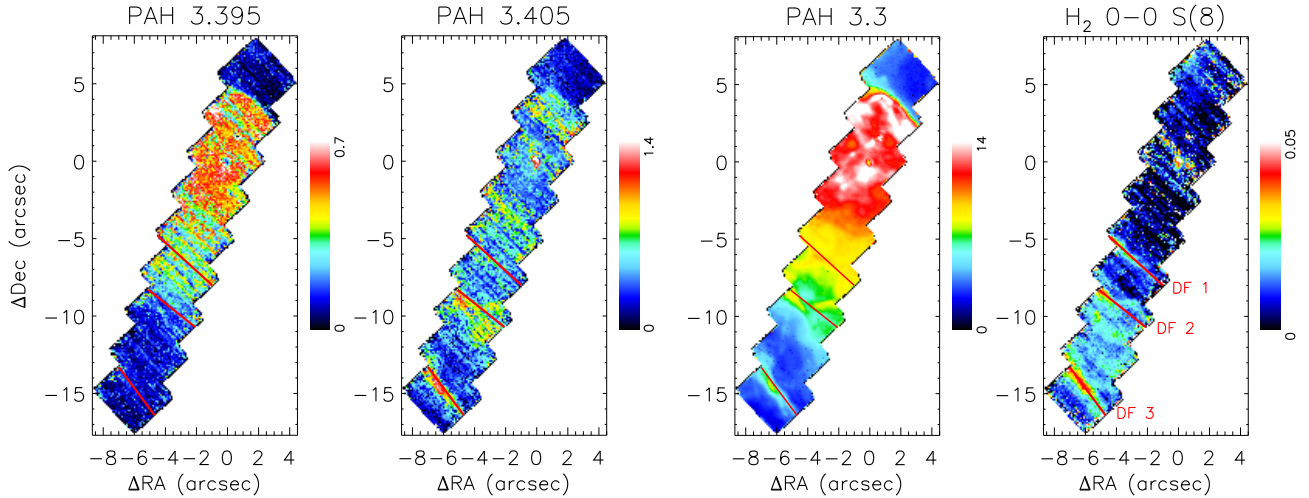


Figure 2. Intensity maps of the PAH 3.395 μm , PAH 3.405 μm , PAH 3.3 μm and H_2 0-0 S(8) emission features in the Orion Bar region ($1''=0.002$ pc). The three dissociation fronts (DF) are indicated in each map. Spaxel fluxes are in units of 10^{-15} ergs s^{-1} cm^{-2} . Typical errors on fluxes are in the range 10–20%, except for H_2 0-0 S(8), where median error is 26%.

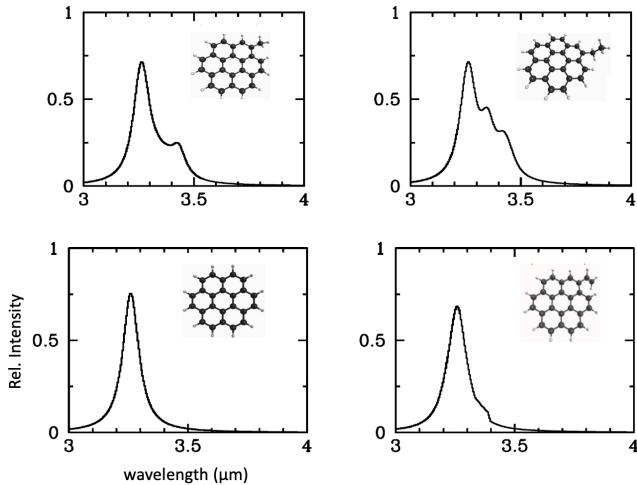


Figure 3. DFT theoretical emission spectra of the 3-4 μm region showing aliphatic and aromatic C-H stretching vibrational modes for molecules with aliphatic side groups. From bottom left and going clockwise, Coronene $\text{C}_{24}\text{H}_{12}$, Coronene with methyl side-group $\text{C}_{24}\text{H}_{11}\text{-CH}_3$, Coronene with ethyl side-group $\text{C}_{24}\text{H}_{11}\text{-CH}_2\text{-CH}_3$, Coronene with vinyl side-group $\text{C}_{24}\text{H}_{11}\text{CH=CH}_2$.

a single feature). Nonetheless, the Red Rectangle, a PN illuminated by HD 44179 of $T_{\text{eff}} \sim 7750$ K, had a rather low PAH 3.4 μm intensity, much lower than that of PDRs and RNs illuminated by stars of much higher T_{eff} (Geballe et al. 1985). This implies that although the hardness of the radiation field is one of the parameters affecting the survival of aliphatic side-groups attached to PAHs it is probably not the only one.

4.1 The case of the Orion Bar

We employ JWST spatially resolved data to further investigate which factors determine the relative strength of the two PAH 3.4 sub-features at 3.395 and 3.405 μm . For this purpose, we first turn to

the JWST/NIRSpec IFU spatially resolved observations of the Orion Bar since its exquisite resolution enables a detailed investigation of the spatial extent of the features. Figure 2 shows the spatially resolved maps of the Orion Bar in the PAH3.3, PAH3.395, PAH3.405 and H_2 0-0 S(8) lines. Similar maps have been presented in Peeters et al. (2024); Schroetter et al. (2024) but for consistency we show our own analysis here. Inspection of the maps in Figure 2 shows that the PAH 3.405 μm feature peaks in regions where the H_2 0-0 S(8) emission is strong, hinting at a possible link between the two. A prominent enhancement in the strength of PAH 3.405 feature is seen at the southern end of the mapped region, coincident with the Dissociation Fronts (DF 2 and 3) discussed in Habart et al. (2023); Peeters et al. (2024) and indicated in our maps as well. Emission from PAH 3.395, on the other hand, dominates in regions which are closer to the Trapezium stars, located towards the north-west (off the map, roughly in the direction of the long axis of the image mosaic). The morphology of the PAH 3.395 μm emission broadly follows that of the PAH 3.3 μm , the latter arising from aromatic C-H stretches which are more robust against destruction by UV photons. The spatial distribution of the two features, therefore, implies that the PAH 3.405 likely arises in regions which are shielded from intense UV radiation, with the molecular H_2 providing the shielding.

A link between PAH emission morphology and that of other dense gas tracers has already been suggested by various studies. Rigopoulou et al. (2002); Roussel et al. (2007); Pereira-Santaella et al. (2010) demonstrate that a strong correlation exists between PAH and the pure H_2 rotational lines. More recently, Alonso-Herrero et al. (2020) investigated the relation between the detection of the PAH 11.3 μm feature in the nuclear regions of Seyfert galaxies and the properties of the cold molecular gas. They found that the strength of PAH 11.3 emission correlates positively with the column density implying that the molecular gas likely plays a role in shielding the PAH molecules in the harsh environments of Seyfert nuclei. The PAH 3.395, on the other hand, traces regions which have been exposed to UV photons as has been suggested by e.g. Schroetter et al. (2024).

In Figure 4 (left) we plot the PAH3.395/PAH3.405 ratio as a function of the PAH3.3/ H_2 0-0 S(8) ratio for the Orion Bar (the H_2 pure rotational line at 5.053 μm). The majority of the spatially resolved points appear to have PAH3.395/PAH3.405 values above ~ 0.3 with

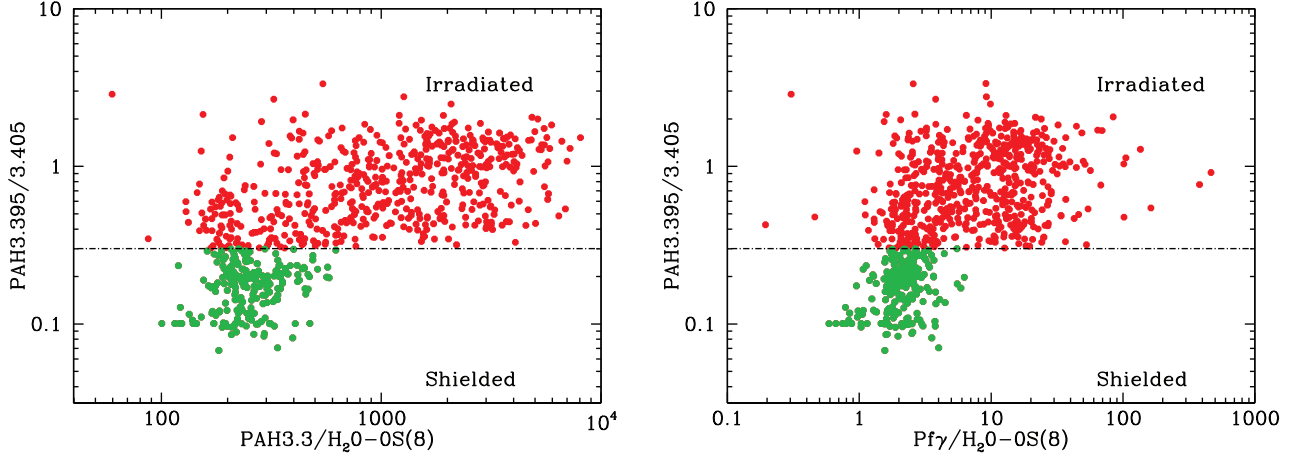


Figure 4. PAH 3.395/3.405 as function of PAH3.3/H₂ flux ratio for the rotational H₂ 0-0 S(8) emission line at $\lambda = 5.05 \mu\text{m}$ (left panel) and the Pfund γ /H₂ ratio (right panel) for the Orion Bar. We assign those points with PAH3.395/3.405 < 0.3 to “shielded” PAHs (green circles) and the remaining points with values above this ratio as “irradiated” PAHs (red circles), as discussed in the text.

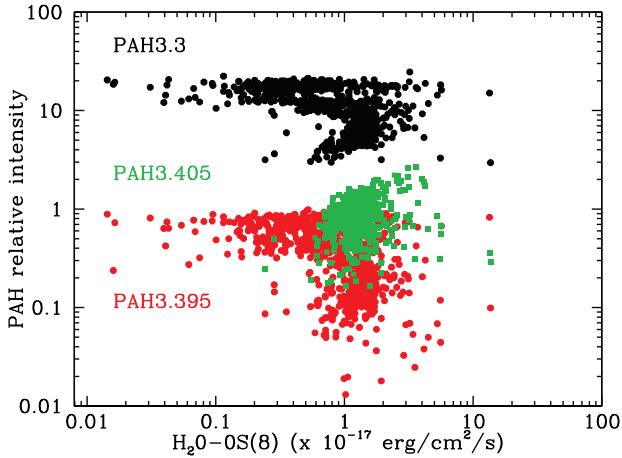


Figure 5. The distribution of the spatially resolved points for the PAH 3.3 (black), 3.395 (red) and 3.405 (green) μm features as a function of the H₂ 0-0 S(8) line, for the Orion Bar.

a median of around 1. Interestingly, there appears to be a cluster of points with low values in the PAH3.395/3.405 ratio, corresponding to PAH molecules with a notably stronger PAH3.405 feature. These points all have PAH3.3/H₂ in the range ~ 100 –750. The upper value of this ratio together with a value for the PAH3.395/3.405 ratio of ~ 0.3 mark a sharp transition into a region which is devoid of any observational points. We interpret the presence of this clear locus of points with PAH3.395/3.405 < 0.3 as evidence of shielding of the more fragile aliphatic PAH molecules, responsible for the 3.405 μm peak, by clouds of molecular hydrogen. As the PAH3.3/H₂ ratio grows bigger (hence the H₂ emission becomes weaker), exposure to FUV photons will tend to destroy some of the fragile aliphatic side chains responsible for the PAH 3.405 emission.

In order to locate the region(s) where PAH 3.395/PAH 3.405 < 0.3 we take the ratio of the PAH 3.395 and PAH 3.405 maps and apply a cut of 0.3 to the ratio values. In this manner, we create a mask which

is shown in Figure A1. The areas with PAH 3.395/PAH 3.405 < 0.3 (shown in green) are coincident with peaks of the H₂ 0-0 S(8) emission (Figure 2) which shows higher intensity in the lower half of the Orion mosaic. These peaks in H₂ emission trace the DF fronts (e.g. Habart et al. 2023; Peeters et al. 2024). In these regions, dissociating FUV photons are attenuated enough to just excite the aliphatic molecules without destroying them. As one moves north of the molecular region past the DF regions, and toward the Trapezium stars, higher UV photon fluxes facilitate the processing of the aliphatic molecules, removing some of the alkylated bands and resulting in a gradual increase in the PAH 3.395/PAH 3.405 ratio. This is also evident in Figure 5 where we plot the spatially resolved points for each of the three PAH features as a function of the strength of the molecular hydrogen line H₂(0–0)S8. It is clear that the PAH 3.405 points cluster around high values of H₂ and whilst the molecules responsible for the PAH 3.395 peak are also present, their emission is weaker. In addition, it appears that the PAH 3.405 intensity increases with increasing H₂ intensity, contrary to the behaviour of both the PAH 3.395 and PAH 3.3 features.

A similar picture emerges when we examine the variation of the PAH sub-features as a function of the ionizing flux (in this case parameterized by the Pf γ line). The right-hand plot of Figure 4 shows PAH 3.395/PAH 3.405 as a function of the Pf γ /H₂ ratio. We observe a similar distribution of the spatially resolved points of the Orion Bar as we saw earlier (in the left-hand side plot of the same figure). We note the existence of a clear cluster of points with values of the ratio of PAH 3.395/PAH 3.405 < 0.3 and Pf γ /H₂ < 10. As before, in these regions the molecular H₂ clouds are shielding the more fragile aliphatic molecules from ionizing photons (as is evident from the low values in the Pf γ /H₂ ratios). Once the Pf γ /H₂ ratio crosses the threshold value of 10, we move to more irradiated regions where the UV field is stronger and where the H₂ molecules are photo-dissociated. In these regions, photo-processing of aliphatic PAHs is likely to take place resulting in large PAH 3.395/PAH 3.405 ratios. The analysis of the Orion Bar data has enabled us, for the first time, to locate regions where fragile PAH molecules are shielded from FUV photons. We were able to trace these regions through the weak 3.405 μm emission of the PAH molecules.

PAH molecules in regions exposed to a hard radiation field exhibit

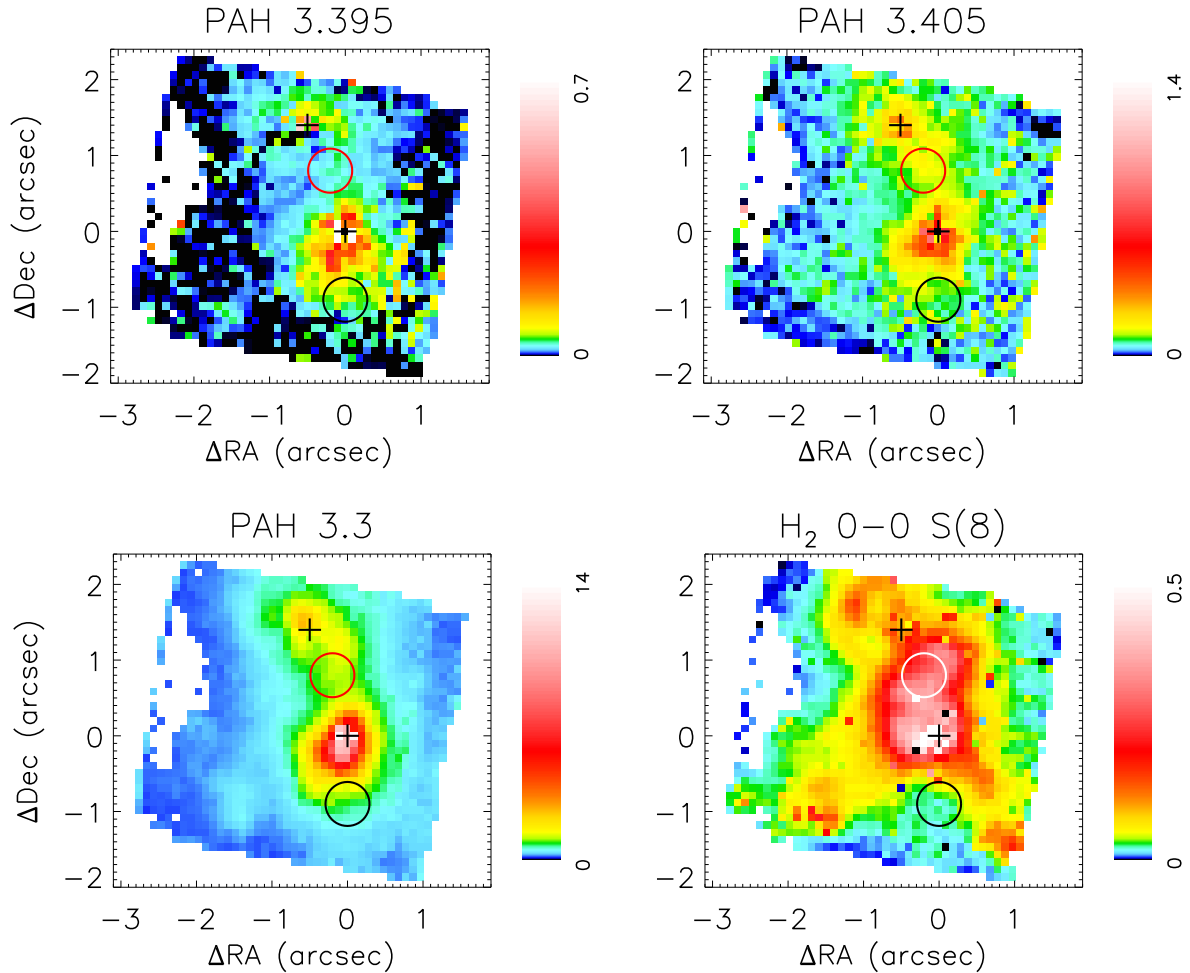


Figure 6. Intensity maps of the PAH 3.395 μm , PAH 3.405 μm , PAH 3.3 μm and H_2 0–0 S(8) emission features in NGC6240 ($1''=524$ pc). The black crosses denote the location of the two nuclei. The red (white for the H_2 0–0 S(8) map) and black circles represent the interaction zone and the region south of the southern nucleus as discussed in the text. Spaxel fluxes are in units of 10^{-15} ergs s^{-1} cm^{-2} . Typical errors on fluxes are in the range 10–20%.

weak 3.405 μm emission, presumably because the fragile aliphatic side chains are destroyed by the energetic FUV photons. These regions are labelled as “irradiated” regions by [Schroetter et al. \(2024\)](#). The presence of dense molecular gas, traced by the H_2 emission, shields the PAH molecules from the energetic FUV photons. This not only softens the radiation field, but also weakens it, so that there is less PAH emission overall. However, as the PAH molecules remain intact, they exhibit all three emission features, at 3.3, 3.395 and 3.405 μm , with PAH 3.405 stronger than PAH 3.395 emission.

4.2 The case of NGC 6240

We now turn to NGC 6240 as we seek to establish whether the same mechanism, where the molecular H_2 is shielding the PAHs from strong UV fields is observed on larger scales in nearby galaxies with strong molecular hydrogen emission, even though the spatial resolution for the NGC 6240 observations is several orders of magnitudes coarser than for the Orion Bar. Figure 6 shows the intensity maps of the PAH 3.3, PAH 3.395, PAH 3.405 and H_2 0–0 S(8) lines in the nuclear region of NGC 6240. The location of the two NGC 6240 nuclei is indicated with crosses on all the images. The morphology of the PAH 3.3 map delineates the regions in the galaxy where the

PAH molecules are excited by FUV photons. Within these regions, we see a strong enhancement of the PAH 3.405 emission relative to the PAH 3.395 emission in the so-called *interaction* region, marked by a red circle in Figure 6. Conversely, little PAH 3.405 emission is seen from the region south of the southern nucleus, indicated by the black circle. The corresponding region in the H_2 emission map shows a “hole”, whereas considerable PAH 3.395 emission is present. The location of this “hole” coincides with the ionized bubble south of the southern nucleus, as identified and discussed in [Ceci et al. 2025](#).

The data points with values of PAH 3.395/PAH 3.405 < 0.3 (the “shielded” region) are all located in the “interaction region” between the two nuclei of NGC 6240. This is coincident with the region where the H_2 molecular hydrogen emission is strong, as has already been noted by [Tecza et al. \(2000\)](#); [Lutz et al. \(2003\)](#); [Ceci et al. \(2025\)](#); [Hermosa Muñoz et al. \(2025\)](#) and is evident in the map shown in Figure 6. This is also consistent with the findings from the analysis of the Orion Bar where the peak of the PAH 3.405 intensity is coincident with regions of high H_2 intensity as shown in Figure 5. Our qualitative interpretation uses the H_2 0–0 S(8) as an indicator of the presence of warm molecular gas, given its proximity in wavelength to the PAH 3.3 features. Although the higher 0–0 S transitions trace warmer gas, we note that in NGC 6240 all the H_2 0–0 transitions

exhibit the same morphology, with a strong peak at the interaction region, in between the two nuclei (Hermosa Muñoz et al. in prep.). We will revisit this issue in the Discussion section.

NGC 6240 is well-known for being H_2 -luminous not only in vibrational lines (e.g. Joseph et al. 1984; Tecza et al. 2000; van der Werf et al. 1993) but also in pure rotational lines. Lutz et al. (2003) found that the luminosity of the H_2 pure rotational lines of $1.8 \times 10^9 L_\odot$ corresponds to 0.3% of the bolometric luminosity of the galaxy. In Figure 7 we plot the ratio of the PAH3.395/PAH3.405 as a function of the PAH3.3/ H_2 0–0 S(8) ratio. The NGC 6240 points broadly follow the same distribution as with the Orion Bar data (Figure 4 left). A fraction of the spatially resolved NGC 6240 data points have low PAH 3.395/PAH 3.405 values (<0.3), these points are indicated with the green symbols in Figure 7. Interestingly, all NGC 6240 data points with low PAH 3.395/PAH 3.405 values have PAH3.3/ H_2 values below 10, and as was the case with the Orion Bar, the bottom right-side portion of the plot is devoid of points. Once again, we see evidence of H_2 molecular gas shielding: the large amount of molecular hydrogen present in NGC 6240 shields the aliphatic PAHs from energetic FUV photons. Following the same procedure as outlined earlier, we create a ‘mask’ for NGC 6240 by dividing the two maps PAH 3.395/PAH 3.405 and applying the same cut of 0.3 for the ratio. The mask is shown in Figure A2, with the two circles marking the “shielded” region and the “irradiated” region overlaid. It is very clear that the PAH 3.405 emission is strong in the shielded region, and weak in the irradiated region, in comparison to the PAH 3.395 emission.

Figure 7 (right) shows the ratio of PAH 3.395/PAH 3.405 as a function of the Pf_γ/H_2 0–0 S(8) ratio. The shape of the distribution of the NGC 6240 points loosely follows that of the Orion Bar but with noticeably more scatter. This is not surprising given that in NGC 6240 the Pf_γ emission is overall stronger and, in particular, around the two nuclei (see e.g., Ceci et al. 2025). Whereas for the Orion Bar there are no points with PAH 3.395/PAH 3.405 <0.3 and $Pf_\gamma/H_2 >10$, in NGC 6240 the H_2 emission lines are almost two orders of magnitude stronger. For the same PAH 3.395/PAH 3.405 ratio, the region devoid of points has $Pf_\gamma/H_2 > 0.05$. As in the case of the Orion Bar, the PAH 3.395/PAH 3.405 ratio increases in regions where the ionizing flux (as traced by Pf_γ) is strong.

It is also worth pointing out that the nominal spatial resolution of the NGC 6240 observations is a lot coarser than that of the Orion Bar, with each spaxel corresponding to 52 pc in linear scale. Therefore, each spaxel in NGC 6240 is sampling much larger areas including a mix of H_2 and PDR regions. The much stronger H_2 emission in NGC 6240, enhanced by the presence of powerful shocks (e.g. Sugai et al. 1997; Lutz et al. 2003), causes the PAH3.3/ H_2 and Pf_γ/H_2 ratios to have lower values than in Orion such that a direct comparison of the ratio ranges is not possible. We also note that the H_2 emission morphology is quite distinct to the PAH emission, as the excitation mechanisms are not the same. The analysis presented here is limited to the regions where PAH 3.3 emission is observed.

Still we note that there are two regions in NGC 6240 that exhibit clear signatures consistent with our hypothesis: (1) the “interaction region” exhibits strong H_2 emission, and a low PAH 3.395/PAH 3.405 ratio, consistent with shielding by dense molecular gas, and (2) the region south of the southern nucleus, showing evidence of stronger UV flux (see figure 21 of Ceci et al. (2025)), little molecular gas emission, and exhibits PAH 3.395 emission, but little or no PAH 3.405. These regions are indicated by red and black circles in Figure 6 respectively.

5 DISCUSSION

The 3.4 μm aliphatic C–H emission has been widely seen in various galactic astrophysical sources (e.g. Sloan et al. 1997; Mori et al. 2014; Pilleri et al. 2015; Boersma et al. 2023). However, the detection of two separate features at 3.395 and 3.405 μm in external galaxies had not been observed prior to JWST. The two features have, so far, been seen in the Orion Bar data (Peeters et al. 2024), and a number of other galactic sources (e.g. Boersma et al. 2023). In their work, Schroetter et al. (2024) employed template spectra to fit the 3.3 and the 3.4 μm PAH bands by fitting single profiles to each of these two features. In contrast, in this work, we fit the two sub-features at 3.4 μm separately with Drude profiles, and the 3.3 μm feature using a combination of Drude and Gaussian profiles, as discussed in Section 2.1.2. Our method results in robust fits for every spaxel in the Orion Bar and NGC 6240. For each of these two targets, through the analysis presented here, we have been able to identify regions where there appears to be an enhanced population of fragile aliphatic PAHs, which are responsible for the PAH 3.405 μm peak. Their survival appears to depend on the presence of dense molecular gas that shields the PAH molecules from energetic UV photons, whilst still allowing lower energy UV photons to excite the PAH molecules.

The comparison of the distribution of aromatic and aliphatic molecules (Figure 5) reveals that the PAH 3.395 emitting molecules follow broadly the distribution of the aromatic ones whereas those responsible for the PAH 3.405 band appear to cluster around high intensity values of the H_2 0–0 S(8) line. The theoretical DFT spectra show that the 3.405 μm peak is prominent when there are $-CH_3$ side-groups attached to the PAH molecule. Given that the aliphatic-to-aromatic (PAH3.4/PAH3.3) ratio decreases with increasing intensity of the FUV radiation field (Sloan et al. 1997; Mori et al. 2014), it is possible that the molecules responsible for the PAH 3.405 μm peak will only survive when they are sufficiently shielded from FUV radiation. This is consistent with observations of an enhancement of PAH 3.405 when the H_2 intensity is high, as shown in Figure 5.

Previous observations of PDRs have also shown that emission from aromatic PAH molecules and that from H_2 excited by fluorescence are nearly co-spatial, with H_2 sometimes seen to extend slightly deeper into molecular clouds (e.g. Sellgren et al. 1990; Tielens et al. 1993; Habart et al. 2003). This co-spatial emission is not unexpected since both species are excited by FUV photons. PAH molecules can also be excited by lower energy photons in the ultraviolet and optical, but with smaller absorption cross sections (see Li & Draine 2001); although FUV photons will always dominate the excitation whenever massive stars or AGN are present. However, H_2 is dissociated by FUV photons between 11.3 and 13.6 eV where it is not self-shielded, whereas aromatic PAHs survive the absorption of these photons.

In the case of relatively dense molecular clouds, PAHs may reside on the surfaces of large grains. When the propagating photoionization/photodissociation front arrives at a parcel of gas that was previously “dark cloud” material, PAHs will be ejected from the grains. This ejection has two main consequences: the PAHs begin to emit following single-photon heating and second, the photoelectric heating rate increases, heating the H_2 gas (e.g., Allers et al. 2005). In this scenario, H_2 emission should peak at slightly higher optical depth than aromatic bands but likely at the same optical depth as the aliphatic PAH 3.405 band.

Can we link the presence of the most fragile aliphatic PAHs, those responsible for the PAH 3.405 μm peak, to the physical conditions of the molecular clouds and in particular the levels of extinction required to shield the PAH molecules? In the case of the Orion Bar,

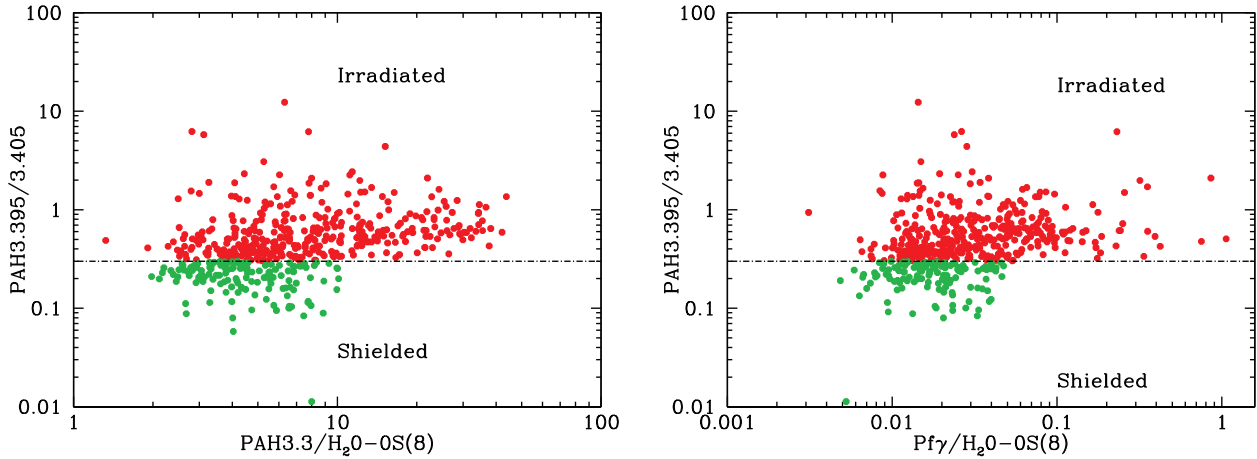


Figure 7. PAH 3.395/3.405 as function of PAH 3.3/H₂O–S(8) for the rotational H₂O–S(8) emission line at $\lambda = 5.05 \mu\text{m}$ (left panel) and the Pfund γ /H₂ ratio (right panel), for NGC 6240. We assign those points with PAH 3.395/3.405 < 0.3 to “shielded” PAHs (green circles) and the remaining points with values above this ratio as “irradiated” PAHs (red circles), as discussed in the text.

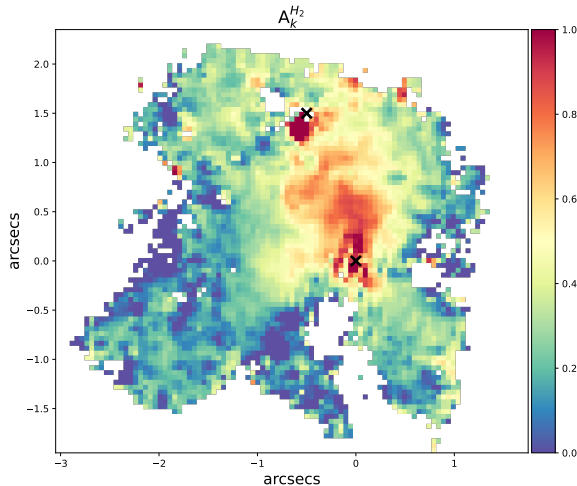


Figure 8. NGC 6240 K band extinction map (A_K) based on H₂ rovibrational lines that share the same upper level (i.e., ν, J)

Peeters et al. (2024) determined that the extinction towards DF3 has values of $A_V \sim 1.8$ to 2.30 mag assuming a screen or mixed dust scenario. Their analysis concluded that the variations seen in the profiles and the ratios of aliphatic to aromatic PAHs are also influenced by changes in the FUV radiation.

A comparison of the maps shown in Figures 6 and A2 reveals that the “shielded” molecules in NGC 6240 are located in the “interaction region” between the two nuclei. Figure 8 shows the A_K extinction map of NGC 6240, assuming a screen dust model. The map was created in a manner similar to that described by Rosenthal et al. (2000), where all detected H₂ vibrational transitions that share the same upper level (ν, J) are used to determine the differential extinction (more details in Speranza et al., in prep). The highest values of the extinction are found towards the southern nucleus of NGC 6240. This region has a value of $A_K \sim 1.0$ mag corresponding to an $A_V \sim 10$ mag. Extinction towards the interaction region is around $A_V \sim 6$ mag. The interaction region is the location where the aliphatic PAH ratio (PAH 3.395/PAH 3.405) is < 0.3, hence this is where the “shielded

PAHs” are located. These PAHs must reside in the outer layers of the molecular clouds. The dense, inner regions of the molecular clouds likely correspond to very high levels of extinction that significantly attenuate the FUV photons, resulting in little or no PAH emission.

Given that in the Orion Bar the extinction towards DF3 was estimated to be $A_V \sim 1.8$ -2.30 mag (Peeters et al. 2024), we conclude that as long as the A_V values remains ≥ 2 , aliphatic molecules are able to survive in the outer layers of molecular clouds, just past the transition zone between atomic and molecular hydrogen gas. It is, however, worth noting that although the extinction towards the Southern nucleus has the highest values, the radiation field is also very strong (e.g., Ceci et al. 2025) potentially destroying the fragile PAH 3.405 molecules.

However, a major difference between the Orion Bar and NGC 6240 is the source of H₂ excitation. While PDRs dominate the excitation of H₂ in the Orion Bar, shocks have been implicated as an extra mechanism for H₂ excitation in NGC 6240, especially in the interaction region (e.g., Tecza et al. 2000; Lutz et al. 2003). An in-depth analysis of the impact of shocks on the PAH population in NGC 6240 is beyond the scope of the present work and will be the focus of a forthcoming study.

6 CONCLUSIONS

The spatially resolved spectroscopic capabilities of JWST/NIRSpec IFU, combined with the telescope’s unprecedented mid-IR sensitivity, has allowed us to clearly identify and analyze two sub-features in the PAH 3.4 μm emission band, both in galactic and extra-galactic sources, for the first time. The PAH 3.4 μm feature most often arises from bond stretches within the aliphatic side-chains attached to aromatic PAH molecules. The two sub-features, the PAH 3.395 μm peak and the PAH 3.405 μm peak, have been observed in the Orion Bar region, with a very strong correlation between the PAH 3.405 emission and the molecular H₂ vibrational emission. The PAH 3.395 emission, on the other hand, follows the morphology of the much brighter PAH 3.3 μm feature, arising from aromatic bond stretches.

Backed up by theoretical PAH spectra computed using DFT, we conclude that the PAH 3.405 sub-feature indicates the presence of fragile aliphatic side-chains of PAH molecules. The thermal emission

is excited by UV photons of ~ 5 eV in energy. However, the presence of stronger UV radiation can cause these side-chains to completely break off. Thus, the presence of strong PAH 3.405 emission, in particular, values of the ratio PAH 3.395/PAH 3.405 < 0.3 , corresponds to regions where the PAH molecules are *shielded* by dense molecular gas, so that only modestly energetic UV photons penetrate to excite the PAHs.

Using spatially resolved plots of PAH 3.395/PAH 3.405 vs. PAH 3.3/H₂ on a spaxel-by-spaxel basis, we show a clear demarcation between shielded and irradiated regions. Strong PAH 3.405 μm emission only arises in regions of high molecular gas density, evidenced by the complete lack of points with low PAH 3.395/PAH 3.405 and high PAH 3.3/H₂. This is true both in the Orion Bar region, but also in NGC 6240, although the spaxels encompass very different size scales in the two sources. In contrast, the PAH 3.395 sub-feature arises from more robust aliphatic side-chains that can withstand irradiation by more energetic UV photons, similar to the aromatic PAH molecules. This *irradiated* aliphatic PAH 3.395 sub-feature displays an almost perfect correlation in its morphology with the PAH 3.3 emission (arising from aromatic PAH molecules), both in the Orion Bar, and in the nuclear region of NGC 6240.

Dense molecular gas is required to shield the fragile aliphatic side-chains that give rise to the PAH 3.405 feature. However, if no UV photons can penetrate, the PAHs are not excited, and do not exhibit thermal emission. Thus, a “Goldilocks” level of shielding, corresponding to A_V of \sim a few, appears to provide the optimal conditions to observe both components of the PAH 3.4 μm feature, leading to a double-peaked emission line. We conclude that the PAH 3.405 μm and PAH 3.395 μm emission features can provide robust diagnostics of the physical conditions of the ISM, and can be exploited to trace the energetics of the photon field penetrating molecular clouds.

ACKNOWLEDGEMENTS

We thank the anonymous referee for perceptive and insightful comments which helped improve the manuscript. NT and DR acknowledge support from STFC through grant ST/W000903/1. FD acknowledges support from STFC through studentship ST/W507726/1. IGB is supported by the Programa Atracción de Talento Investigador “César Nombela” via grant 2023-T1/TEC-29030 funded by the Community of Madrid. AAH and LHM acknowledge financial support by grant PID2021-124665NB-I00 funded by the Spanish Ministry of Science and Innovation and the State Agency of Research MCIN/AEI/10.13039/501100011033, PID2021-124665NB-I00 and ERDF A way of making Europe. MPS acknowledges support under grants RYC2021-033094-I, CNS2023-145506 and PID2023-146667NB-I00 funded by MCIN/AEI/10.13039/501100011033 and the European Union NextGenerationEU/PRTR.

Computational resources were provided by the Advanced Research Computing (ARC) facility at the University of Oxford [1]. We gratefully acknowledge the use of ARC for supporting the quantum chemical calculations performed in this work.

This work is based on observations made with the NASA/ESA/CSA James Webb Space Telescope. The data were obtained from the Mikulski Archive for Space Telescopes at the Space Telescope Science Institute, which is operated by the Association of Universities for Research in Astronomy, Inc., under NASA contract NAS 5-03127 for JWST; and from the European JWST archive (eJWST) operated by the ESAC Science Data Centre (ESDC) of the European Space Agency. These observations are associated with programs #1328 and #1670.

DATA AVAILABILITY

The JWST data used in this work are publicly available as part of DD-ERS Program 1288 (PI: O. Berne), and GTO1 - Program 1265 (PI: A. Alonso-Herrero) and downloadable from the MAST archive.

REFERENCES

- Allamandola L. J., Tielens A. G. G. M., Barker J. R., 1985, *ApJ*, **290**, L25
 Allers K. N., Jaffe D. T., Lacy J. H., Draine B. T., Richter M. J., 2005, *ApJ*, **630**, 368
 Alonso-Herrero A., et al., 2014, *MNRAS*, **443**, 2766
 Alonso-Herrero A., et al., 2020, *A&A*, **639**, A43
 Barker J. R., Allamandola L. J., Tielens A. G. G. M., 1987, *ApJ*, **315**, L61
 Barzaga R., et al., 2025, *arXiv e-prints*, p. arXiv:2511.04606
 Berné O., et al., 2022, *PASP*, **134**, 054301
 Boersma C., et al., 2023, *ApJ*, **959**, 74
 Buragohain M., Pathak A., Sakon I., Onaka T., 2020, *ApJ*, **892**, 11
 Cabezas C., et al., 2025, *arXiv e-prints*, p. arXiv:2508.13857
 Ceci M., et al., 2025, *A&A*, **695**, A116
 Chen Y.-C., et al., 2024, *ApJ*, **968**, 92
 Chiar J. E., Tielens A. G. G. M., Adamson A. J., Ricca A., 2013, *ApJ*, **770**, 78
 Chown R., et al., 2024, *A&A*, **685**, A75
 Donnan F. R., García-Bernete I., Rigopoulou D., Pereira-Santaella M., Alonso-Herrero A., Roche P. F., Hernán-Caballero A., Spoon H. W. W., 2023, *MNRAS*, **519**, 3691
 Draine B. T., Li A., 2007, *ApJ*, **657**, 810
 Draine B. T., Li A., Hensley B. S., Hunt L. K., Sandstrom K., Smith J. D. T., 2021, *ApJ*, **917**, 3
 Duley W. W., Williams D. A., 1981, *MNRAS*, **196**, 269
 Galliano F., Madden S. C., Tielens A. G. G. M., Peeters E., Jones A. P., 2008, *ApJ*, **679**, 310
 García-Bernete I., et al., 2022, *A&A*, **666**, L5
 García-Bernete I., Pereira-Santaella M., González-Alfonso E., Rigopoulou D., Efstathiou A., Donnan F. R., Thatte N., 2024a, *A&A*, **682**, L5
 García-Bernete I., et al., 2024b, *A&A*, **691**, A162
 Geballe T. R., Lacy J. H., Persson S. E., McGregor P. J., Soifer B. T., 1985, *ApJ*, **292**, 500
 Habart E., Boulanger F., Verstraete L., Pineau des Forêts G., Falgarone E., Abergel A., 2003, *A&A*, **397**, 623
 Habart E., et al., 2023, *A&A*, **673**, A149
 Hermosa Muñoz L., et al., 2025, *A&A*, **693**, A321
 Hernandez S., et al., 2023, *ApJ*, **948**, 124
 Hrivnak B. J., Geballe T. R., Kwok S., 2007, *ApJ*, **662**, 1059
 Imanishi M., Nakagawa T., Shirahata M., Ohshima Y., Onaka T., 2010, *ApJ*, **721**, 1233
 Joseph R. D., Wade R., Wright G. S., 1984, *Nature*, **311**, 132
 Jourdain de Muizon M., D’Hendecourt L. B., Geballe T. R., 1990, *A&A*, **227**, 526
 Kerkeni B., García-Bernete I., Rigopoulou D., Tew D. P., Roche P. F., Clary D. C., 2022, *MNRAS*, **513**, 3663
 Lai T. S. Y., et al., 2023, *ApJ*, **957**, L26
 Leger A., Puget J. L., 1984, *A&A*, **137**, L5
 Li A., Draine B. T., 2001, *ApJ*, **554**, 778
 Li A., Draine B. T., 2012, *ApJ*, **760**, L35
 Lutz D., Sturm E., Genzel R., Spoon H. W. W., Moorwood A. F. M., Netzer H., Sternberg A., 2003, *A&A*, **409**, 867
 Lyu J., Yang X., Li A., Sun F., Rieke G. H., Albers S., Shivaee I., 2025, *arXiv e-prints*, p. arXiv:2502.18464
 Mori T. I., Onaka T., Sakon I., Ishihara D., Shimonishi T., Ohsawa R., Bell A. C., 2014, *ApJ*, **784**, 53
 Ohsawa R., Onaka T., Sakon I., Matsuura M., Kaneda H., 2016, *AJ*, **151**, 93
 Pauzat F., Talbi D., Ellinger Y., 1999, *MNRAS*, **304**, 241
 Peeters E., et al., 2024, *A&A*, **685**, A74
 Pendleton Y. J., et al., 2025, *arXiv e-prints*, p. arXiv:2508.12601

- Pereira-Santaella M., Alonso-Herrero A., Rieke G. H., Colina L., Díaz-Santos T., Smith J. D. T., Pérez-González P. G., Engelbracht C. W., 2010, *ApJS*, **188**, 447
- Perna M., et al., 2024, *A&A*, **690**, A171
- Pilleri P., Joblin C., Boulanger F., Onaka T., 2015, *A&A*, **577**, A16
- Ramos Almeida C., et al., 2025, *arXiv e-prints*, p. [arXiv:2504.01595](https://arxiv.org/abs/2504.01595)
- Ricca A., Bauschlicher Jr. C. W., Boersma C., Tielens A. G. G. M., Allamandola L. J., 2012, *ApJ*, **754**, 75
- Rigopoulou D., Spoon H. W. W., Genzel R., Lutz D., Moorwood A. F. M., Tran Q. D., 1999, *AJ*, **118**, 2625
- Rigopoulou D., Kunze D., Lutz D., Genzel R., Moorwood A. F. M., 2002, *A&A*, **389**, 374
- Rigopoulou D., et al., 2021, *MNRAS*, **504**, 5287
- Rigopoulou D., et al., 2024, *MNRAS*, **532**, 1598
- Roche P. F., Lucas P. W., Hoare M. G., Aitken D. K., Smith C. H., 1996, *MNRAS*, **280**, 924
- Rosenthal D., Bertoldi F., Drapatz S., 2000, *A&A*, **356**, 705
- Roussel H., et al., 2007, *ApJ*, **669**, 959
- Sandford S. A., Allamandola L. J., Tielens A. G. G. M., Sellgren K., Tapia M., Pendleton Y., 1991, *ApJ*, **371**, 607
- Sandford S. A., Bernstein M. P., Materese C. K., 2013, *ApJS*, **205**, 8
- Schroetter I., et al., 2024, *A&A*, **685**, A78
- Sellgren K., Tokunaga A. T., Nakada Y., 1990, *ApJ*, **349**, 120
- Sloan G. C., Bregman J. D., Geballe T. R., Allamandola L. J., Woodward E., 1997, *ApJ*, **474**, 735
- Smith J. D. T., et al., 2007, *ApJ*, **656**, 770
- Spilker J. S., et al., 2023, *Nature*, **618**, 708
- Sugai H., Malkan M. A., Ward M. J., Davies R. I., McLean I. S., 1997, *ApJ*, **481**, 186
- Tecza M., Genzel R., Tacconi L. J., Anders S., Tacconi-Garman L. E., Thatte N., 2000, *ApJ*, **537**, 178
- Tielens A. G. G. M., 2008, *ARA&A*, **46**, 289
- Tielens A. G. G. M., Meixner M. M., van der Werf P. P., Bregman J., Tauber J. A., Stutzki J., Rank D., 1993, *Science*, **262**, 86
- Weingartner J. C., Draine B. T., 2001, *ApJS*, **134**, 263
- Wexler A., 1967, *Applied Spectroscopy Reviews*, **1**, 29
- Yang X. J., Li A., 2023, *ApJS*, **268**, 50
- Yang X. J., Glaser R., Li A., Zhong J. X., 2013, *ApJ*, **776**, 110
- Yang X. J., Li A., Glaser R., 2020, *ApJS*, **247**, 1
- Zhang L., et al., 2024, *ApJ*, **975**, L2
- van der Werf P. P., Genzel R., Krabbe A., Blietz M., Lutz D., Drapatz S., Ward M. J., Forbes D. A., 1993, *ApJ*, **405**, 522

APPENDIX A: SHIELDED REGIONS

For the Orion Bar and NGC 6240 observations, We present "masks" that show the regions where the PAH 3.395/PAH 3.405 ratio is <0.3 , corresponding to regions where the PAH molecules are "shielded" from energetic UV photons by dense molecular gas.

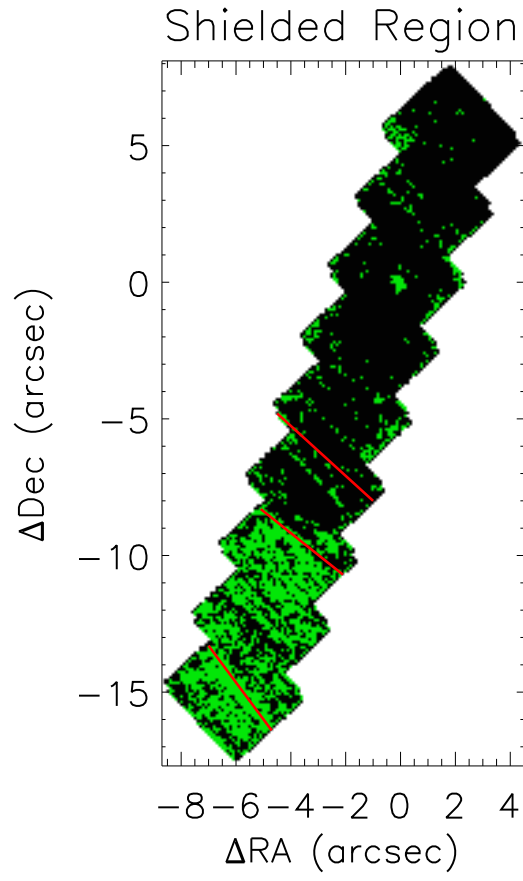


Figure A1. The Orion Bar mask, green areas represent spaxels with PAH 3.395/3.405 values of <0.3 corresponding to "shielded" PAHs, as discussed in the text. The red lines mark the dissocation fronts.

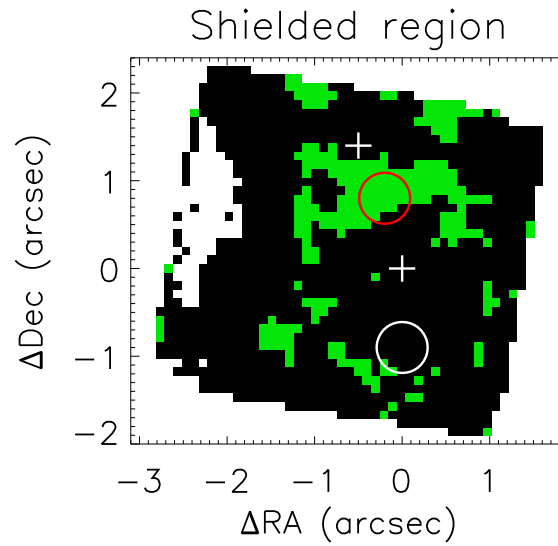


Figure A2. The NGC 6240 mask, green areas represent spaxels with PAH 3.395/3.405 values of <0.3 corresponding to "shielded" PAHs, as discussed in the text. The white crosses mark the locations of the two nuclei. The two circles mark the same regions as in Figure 6, except that the black circle has become white, to make it visible. The red circle corresponds to a "shielded" region, whereas the white circle marks an "irradiated" region.